Article

Morphology-Dependent Transport Potential and Sedimentary Distribution of Microplastics in an Abyssal Pacific Basin

Hua Deng, Yutao Fu, Daohua Chen, Bo Hu, Jiawei Kang and Yinan Deng

No. of pages: **15**
No. of texts: **3**
No. of tables: **5**
No. of Figures:**2**

Text S1: The measured DO concentration was first converted from mass concentration to molar concentration:

$$[O_2]_{\text{meas}} = \frac{DO \times 1000}{M_{O_2} \times \rho} \quad \text{(S1)}$$

where $[O_2]_{\text{meas}}$ is the shipboard-measured DO concentration (μmol/kg), DO is the measured dissolved oxygen concentration (mg/L), M_{O_2} is the molar mass of oxygen, 31.998 g/mol, and ρ is seawater density (kg/L). DO was measured by iodometric titration using an automated titration system (SI TITRONIC 300, Germany). The measured DO concentration was converted from mg/L to μmol/kg using seawater density calculated from the WOA23 temperature and salinity values assigned to each sampling station and depth. This conversion allowed oxygen data to be compared with hydrographic and biogeochemical variables on a mass-normalized basis.

Text S2: Temperature and salinity values used in the density calculations were obtained from WOA23 at the locations and sampling depths of W_1 and W_2. σ_θ referenced to the sea surface was then calculated using EOS-80. To characterize water-mass structure without the influence of hydrostatic compression, potential density was calculated using the international equation of state of seawater, EOS-80. The density of pure water was first expressed as a function of temperature:

$$\rho_w = a_0 + a_1 T + a_2 T^2 + a_3 T^3 + a_4 T^4 + a_5 T^5 \quad \text{(S2)}$$

where ρ_w is the density of pure water, T is temperature, and $a_0 - a_5$ are EOS-80 coefficients.

Seawater density at the reference pressure of 0 dbar was then calculated by incorporating salinity-dependent terms:

$$\rho(S,T,0) = \rho_w + AS + BS^{1.5} + CS^2 \quad \text{(S3)}$$

In Equation S3, the coefficients A, B, and C were parameterized as temperature power series defined by Fofonoff and Millard (1983). Finally, the potential density was derived as the density anomaly relative to the pure water standard:

$$\sigma_\theta = \rho_\theta - 1000 \quad \text{(S4)}$$

where ρ_θ is potential density referenced to the sea surface, and σ_θ is the potential density anomaly (kg/m^3). In this study, σ_θ was used together with AOU to identify stratified water masses and to evaluate whether MP abundance maxima coincided with physical or biogeochemical transition layers.

References

Fofonoff, N.P., Millard, R.C., 1983. Algorithms for computation of fundamental properties of seawater. UNESCO Technical Papers in Marine Science, 53pp.

Text S3: Morphology-dependent sinking velocities were estimated separately for fibers and non-fibrous particles. Observed MP abundance was corrected using the profile-specific FTIR-confirmed synthetic-polymer fraction:

$$C_{\mathrm{corr}} = C_{\mathrm{obs}} \times f_{\mathrm{syn}} \tag{S1}$$

where C_{corr} is the FTIR-corrected MP abundance (items/L), C_{obs} is the observed MP abundance (items/L), and f_{syn} is the confirmed synthetic-polymer fraction from FTIR analysis. In this study, f_{syn} was 0.606 for W_1 and 0.473 for W_2.

For fragments, pellets, and films, the projected-area equivalent radius (r_{eq}, m) was calculated from the measured long (L, m) and short axes (W, m):

$$r_{\mathrm{eq}} = \frac{\sqrt{L \times W}}{2} \tag{S2}$$

The terminal sinking velocity of non-fibrous particles was then estimated using a shape-corrected modified Stokes equation:

$$V_{s,\mathrm{nonfiber}} = \frac{2}{9} \times \frac{(\rho_p - \rho_f) g r_{\mathrm{eq}}^2}{\mu C_{\mathrm{shape}} C_{\mathrm{drag}}} \tag{S3}$$

where $V_{s,\mathrm{nonfiber}}$ is the non-fiber sinking velocity (m/s), ρ_p is the density of the synthetic polymer (kg/m^3), ρ_f is the in situ seawater density (kg/m^3)), g is gravitational acceleration (9.81 m/s^2, μ is seawater dynamic viscosity (Pa·s)), C_{shape} is the morphology-specific shape correction factor, and C_{drag} is the conservative drag multiplier. Shape correction factors were set to 3 for fragments, 1.5 for pellets, and 10 for films. The primary conservative scenario used $C_{\mathrm{drag}} = 2$ to reduce potential overestimation from idealized particle-settling assumptions. Additional drag-sensitivity scenarios used multipliers of 1.5 and 3.0. The drag ×2 scenario was retained as the primary intermediate-conservative case because it reduced the modelled sinking velocity and transport potential relative to the unscaled and drag ×1.5 scenarios (Table

S5).

For fibers, aspect ratio was calculated from measured length and diameter:

$$AR = \frac{L}{d_f} \tag{S4}$$

where AR is the aspect ratio, L is the fiber length (m), and d_f is the fiber diameter, represented by the measured short axis (m). Sinking velocity was estimated using a low-Reynolds-number slender-particle approximation incorporating aspect-ratio, orientation, and drag corrections:

$$V_{s,\text{fiber}} = \frac{(\rho_p - \rho_f) g d_f^2}{18\mu} \times \frac{\ln(AR) + 0.193}{C_{\text{orient}} C_{\text{drag}}} \tag{S5}$$

where $V_{s,\text{fiber}}$ is the fiber sinking velocity (m/s), d_f is the measured fiber diameter (m), C_{orient} is the orientation/tortuosity correction factor, and C_{drag} is the conservative drag multiplier. In this study, C_{orient} was set to 5 to account for non-vertical settling orientation and irregular motion of elongated fibers, and the primary conservative scenario used $C_{\text{drag}} = 2$. An independent empirical distribution of fiber orientation was not available; therefore, orientation sensitivity was represented by the fixed correction factor rather than by a separate probabilistic analysis.

Instantaneous sinking velocities in m/s were converted to daily sinking velocities as:

$$V_{s,d} = V_s \times 86400 \tag{S6}$$

where $V_{s,d}$ is the daily sinking velocity (m/d).

Flux aggregation was performed separately for fibers and non-fibrous particles. At each depth, the observed particle fraction of each morphology group was used to partition the FTIR-corrected abundance:

$$f_{\text{fiber}} = \frac{n_{\text{fiber}}}{n_{\text{total}}} \tag{S7}$$

$$f_{\text{nonfiber}} = \frac{n_{\text{nonfiber}}}{n_{\text{total}}} \tag{S8}$$

where f_{fiber} and f_{nonfiber} are the particle fractions of fibers and non-fibers, respectively, and n is the number of measured particles at a given CTD depth.

Group-specific vertical fluxes were calculated as:

$$F_{\text{fiber}} = C_{\text{corr}} \times f_{\text{fiber}} \times \overline{V}_{s,d,\text{fiber}} \times 1000 \tag{S9}$$

$$F_{\text{nonfiber}} = C_{\text{corr}} \times f_{\text{nonfiber}} \times \overline{V}_{s,d,\text{nonfiber}} \times 1000 \tag{S10}$$

where F_{fiber} and F_{nonfiber} are the morphology-specific vertical fluxes (items/m^2/d), and $\overline{V}_{s,d}$ is the group-specific mean daily sinking velocity (m/d). The factor 1000 converts abundance from items/L to items/m^3.

The total vertical flux at each depth was then calculated as the sum of the fiber and non-fiber fluxes:

$$F_{\text{total}} = F_{\text{fiber}} + F_{\text{nonfiber}} . \tag{S11}$$

Because this morphology-resolved aggregation avoids pooling fibers and non-fibers before velocity averaging, it preserves their distinct hydrodynamic behaviors; the resulting fluxes should therefore be interpreted as conservative, morphology-resolved vertical transport potentials rather than direct sediment-trap measurements.

Table S1. Sampling stations, geographic coordinates, and sampling categories in the western Pacific Pigafetta Basin.

Station	Longitude (°E)	Latitude (°N)	Sampling category
S_1	160.562	16.776	
S_2	161.205	16.657	
S_3	159.366	14.042	
S_4	158.895	13.829	
S_5	157.913	14.548	
S_6	158.445	14.169	
S_7	158.602	14.225	
S_8	158.726	14.268	
S_9	159.017	14.292	
S_{10}	156.928	13.894	
S_{11}	157.489	13.485	
S_{12}	157.648	13.608	
S_{13}	158.545	13.446	
S_{14}	157.957	13.927	
S_{15}	157.453	14.302	
S_{16}	157.976	14.855	
S_{17}	160.253	16.073	Surface sediment
S_{18}	159.782	15.377	
S_{19}	161.197	18.194	
S_{20}	160.822	18.687	
S_{21}	161.935	18.455	
S_{22}	162.260	18.521	
S_{23}	162.734	17.936	
S_{24}	162.003	17.977	
S_{25}	162.596	17.623	
S_{26}	161.479	17.368	
S_{27}	161.713	18.916	
S_{28}	161.126	19.252	
S_{29}	157.099	14.048	
S_{30}	160.709	18.997	
S_{31}	158.198	13.773	
S_{32}	158.956	14.777	
S_{33}	159.325	14.504	
W_1	161.293	18.189	Water-column CTD
W_2	159.282	15.695	

Table S2. Depth-resolved hydrographic and biogeochemical properties and microplastic abundance along two full-depth water-column profiles in the western Pacific Pigafetta Basin.

Sample ID	Depth (m)	DO (mg/L)	TA (mmol/L)	pH	SiO_3^{2-}-Si (μmol/L)	PO_4^{3-}-P (μmol/L)	NH_4^+-N (μmol/L)	NO_2^--N (μmol/L)	NO_3^--N (μmol/L)	AOU (μmol/kg)	σ_θ (kg/m^3)	Dynamic viscosity (Pa·s)	MP abundance (items/L)	Temperature (℃)	Salinity
W_1-01	0	6.0	2.41	8.04	-	0.08	-	-	5.3	16.2	22.3	9.01E-04	3.2 ± 0.3	27.7	34.8
W_1-02	10	6.0	2.39	8.02	-	0.09	-	0.02	0.4	14.6	22.3	9.02E-04	5.2 ± 0.6	27.6	34.8
W_1-03	20	6.1	2.43	8.02	-	0.1	-	-	-	13.5	22.3	9.03E-04	1.7 ± 0.6	27.6	34.8
W_1-04	30	6.0	2.40	8.02	-	0.08	-	-	2.6	14.7	22.3	9.03E-04	4.6 ± 2.3	27.6	34.9
W_1-05	50	5.9	2.40	8.01	-	0.08	-	0.01	2.8	18.1	22.4	9.07E-04	3.4 ± 0.7	27.4	34.9
W_1-06	75	6.1	2.47	8.03	-	0.07	-	0.01	4.3	14.2	22.6	9.14E-04	2.5 ± 1.0	27.1	35.0
W_1-07	100	6.0	2.40	8.01	-	0.1	-	-	-	18.2	22.8	9.25E-04	2.1 ± 0.8	26.5	35.1
W_1-08	150	5.9	2.43	8.02	-	0.1	-	0.28	-	28.6	23.5	9.71E-04	3.0 ± 2.1	24.3	35.1
W_1-09	200	5.4	2.42	8.01	-	0.3	-	0	11.8	57.6	24.4	1.05E-03	6.8 ± 3.8	20.8	35.0
W_1-10	250	5.7	2.38	7.99	0.2	0.5	-	0.03	22.5	62.2	25.0	1.14E-03	3.2 ± 0.5	17.7	34.8
W_1-11	300	6.0	2.42	7.99	4.9	0.8	-	0	37.0	66.1	25.4	1.21E-03	4.4 ± 1.8	15.1	34.6
W_1-12	400	5.2	2.39	7.94	18.4	1.5	-	-	73.7	115.6	26.1	1.37E-03	3.6 ± 0.6	10.6	34.3
W_1-13	500	3.6	2.38	7.87	44.8	2.3	0.02	-	108.8	181.1	26.7	1.48E-03	6.5 ± 2.7	7.8	34.2
W_1-14	600	2.5	2.41	7.83	63.3	2.8	0.05	-	120.7	225.3	27.0	1.55E-03	2.1 ± 0.3	6.3	34.3
W_1-15	700	2.7	2.43	7.83	70.9	2.9	-	-	141.8	222.9	27.1	1.58E-03	2.3 ± 1.4	5.7	34.4
W_1-16	800	2.7	2.45	7.86	79.7	2.9	-	-	140.0	225.1	27.2	1.61E-03	3.1 ± 1.0	5.1	34.5
W_1-17	900	2.8	2.45	7.82	86.3	3.0	-	0.02	142.7	226.8	27.3	1.64E-03	2.6 ± 1.5	4.6	34.5
W_1-18	1000	2.7	2.45	7.82	96.0	3.0	0.01	-	149.4	231.4	27.4	1.66E-03	1.4 ± 0.7	4.2	34.5
W_1-19	1500	3.4	2.49	7.85	125.9	3.0	0.09	-	156.6	220.9	27.6	1.73E-03	1.2 ± 0.4	2.8	34.6
W_1-20	2000	3.7	2.52	7.82	138.8	2.9	-	-	138.5	217.2	27.7	1.78E-03	1.9 ± 1.4	2.1	34.6
W_1-21	3000	4.9	2.52	7.82	142.6	2.8	-	-	126.1	187.3	27.8	1.81E-03	1.6 ± 0.9	1.6	34.7
W_1-22	4000	5.2	2.52	7.85	140.1	2.7	0.05	-	114.9	179.3	27.8	1.81E-03	1.6 ± 0.6	1.5	34.7
W_1-23	5000	5.9	2.54	7.84	128.1	2.6	0.08	0	124.7	158.3	27.8	1.82E-03	2.1 ± 1.8	1.4	34.7
W_1-24	5650	6.2	2.52	7.85	126.2	2.6	0.05	-	129.6	149.0	27.8	1.82E-03	1.3 ± 0.7	1.4	34.7
W_2-01	0	5.6	2.40	8.05	-	0.06	0.12	0.01	1.6	24.6	21.9	8.86E-04	7.8 ± 2.8	28.4	34.7
W_2-02	10	6.2	2.39	8.03	-	0.07	-	0.02	-	7.5	21.9	8.87E-04	4.7 ± 0.9	28.4	34.7

W_2-03	20	6.2	2.42	8.03	-	0.07	-	-	1.2	7.5	21.9	8.88E-04	3.6 ± 0.9	28.4	34.7
W_2-04	30	5.8	2.42	8.03	-	0.1	-	0	-	18.6	21.9	8.88E-04	4.5 ± 2.1	28.4	34.7
W_2-05	50	6.0	2.39	8.02	-	0.06	-	0.01	-	12.5	22.0	8.90E-04	4.5 ± 2.9	28.3	34.7
W_2-06	75	5.6	2.39	8.04	-	0.05	-	0	-	25.8	22.1	8.96E-04	1.7 ± 0.6	27.9	34.8
W_2-07	100	6.0	2.45	8.03	-	0.1	-	0.02	-	17.6	22.4	9.08E-04	3.8 ± 1.8	27.4	34.9
W_2-08	150	6.0	2.48	8.03	-	0.1	-	0.1	-	23.6	23.3	9.53E-04	2.6 ± 0.8	25.2	35.1
W_2-09	200	5.5	2.38	8.04	-	0	-	0.03	8.1	54.3	24.3	1.05E-03	2.7 ± 0.6	21.1	35.0
W_2-10	250	5.3	2.35	8.04	-	1	-	0.03	23.0	76.7	25.1	1.16E-03	1.5 ± 0.6	16.9	34.7
W_2-11	300	5.4	2.33	8.05	3.9	1	-	0.01	47.8	90.2	25.6	1.26E-03	3.4 ± 1.0	13.8	34.4
W_2-12	400	4.8	2.34	8.01	24.7	2	-	-	91.0	131.7	26.3	1.41E-03	1.5 ± 0.6	9.7	34.3
$W_2$13	500	3.6	2.43	7.99	43.2	3	-	-	136.6	185.2	26.7	1.51E-03	3.4 ± 2.3	7.3	34.3
W_2-14	600	2.3	2.38	7.98	58.9	3	0.06	0.01	158.1	228.8	27.1	1.55E-03	3.7 ± 1.1	6.3	34.4
W_2-15	700	2.5	2.47	7.93	69.3	3	-	-	177.0	229.0	27.2	1.58E-03	3.3 ± 1.1	5.7	34.5
W_2-16	800	2.4	2.42	7.91	75.6	3	0.03	-	169.9	233.2	27.3	1.61E-03	2.9 ± 0.6	5.2	34.5
W_2-17	900	2.6	2.46	7.92	81.9	3	0.08	0.02	159.1	232.0	27.3	1.63E-03	1.7 ± 0.3	4.7	34.5
W_2-18	1000	2.7	2.43	7.92	89.8	3	0.08	0.02	174.6	231.9	27.4	1.65E-03	3.0 ± 1.8	4.3	34.5
W_2-19	1500	3.1	2.45	7.94	121.8	3	0.01	-	164.1	230.8	27.6	1.73E-03	2.8 ± 1.3	2.9	34.6
W_2-20	2000	3.4	2.45	7.93	134.7	3	0.04	-	158.5	228.1	27.7	1.77E-03	3.9 ± 1.8	2.1	34.6
W_2-21	3000	4.1	2.48	7.90	139.4	3	0.08	0.02	158.3	208.7	27.7	1.80E-03	3.0 ± 2.9	1.7	34.7
W_2-22	4000	4.8	2.34	7.88	132.2	3	0.08	0	145.2	191.7	27.8	1.81E-03	2.2 ± 0.6	1.5	34.7
W_2-23	5000	5.5	2.42	7.85	124.3	3	0.07	-	141.9	169.3	27.8	1.82E-03	1.2 ± 0.2	1.4	34.7
W_2-24	5650	5.8	2.47	7.85	122.1	3	0.09	0	143.4	159.0	27.8	1.82E-03	0.7 ± 0.4	1.4	34.7

Note: "-" indicates not detected or below the method detection limit. Temperature and salinity were obtained from the annual WOA23 climatology using the nearest horizontal grid cell and nearest available depth level for each profile. AOU and potential density anomaly are therefore climatology-assisted derived variables rather than fully synoptic in situ observations. Dissolved oxygen was measured during the cruise, whereas oxygen saturation was calculated from the WOA23 temperature and salinity values.

Table S3. Physicochemical properties and microplastic abundance of surface sediments collected from the western Pacific Pigafetta Basin.

Station ID	pH	Eh (mV)	Measurement temperature (°C)	MP abundance (items/kg *dw*)
S_1	7.01	579	22.8	128.5 ± 104.4
S_2	7.04	550	22.4	107.5 ± 40.4
S_3	7.24	599	22.1	56.9 ± 15.7
S_4	7.08	537	21.6	18.9 ± 15.2
S_5	6.90	530	20.5	13.1 ± 18.5
S_6	7.14	534	21.2	50.3 ± 31.4
S_7	6.94	547	22.3	12.5 ± 8.9
S_8	7.27	551	22.8	83.2 ± 57.1
S_9	7.06	559	23.9	45.6 ± 36.8
S_{10}	7.06	563	19.8	31.0 ± 31.9
S_{11}	7.11	553	21.0	51.5 ± 8.2
S_{12}	7.20	530	21.9	102.2 ± 53.4
S_{13}	7.27	538	22.1	25.4 ± 36.0
S_{14}	7.17	550	21.8	50.3 ± 23.0
S_{15}	7.12	561	20.8	49.5 ± 23.2
S_{16}	7.09	556	20.2	75.9 ± 32.2
S_{17}	7.15	565	21.4	82.5 ± 31.6
S_{18}	7.17	570	20.1	38.6 ± 27.4
S_{19}	7.20	558	20.3	84.6 ± 48.9
S_{20}	7.21	556	20.2	6.5 ± 9.2
S_{21}	7.23	567	20.1	64.0 ± 40.7
S_{22}	7.22	607	20.3	164.2 ± 64.0
S_{23}	7.24	605	20.0	51.6 ± 8.5
S_{24}	7.25	578	20.5	180.1 ± 102.8
S_{25}	7.23	571	20.4	109.6 ± 71.0
S_{26}	7.21	573	20.3	108.2 ± 39.5
S_{27}	7.19	572	20.4	130.2 ± 107.2
S_{28}	7.25	575	20.7	25.2 ± 8.7
S_{29}	7.22	562	20.4	57.3 ± 1.6
S_{30}	7.28	609	20.1	68.8 ± 49.5
S_{31}	7.27	579	20.6	24.6 ± 17.4
S_{32}	7.25	578	20.3	56.9 ± 25.9
S_{33}	7.20	580	20.2	67.7 ± 34.7

Note: Eh, oxidation–reduction potential; MP, microplastic; dw, dry weight. MP abundance is expressed as mean ± standard deviation of replicate measurements. Sediment pH and Eh were measured at the temperatures listed in the table.

Table S4. Depth-resolved morphology-specific sinking velocities and modelled free-particle vertical transport potentials at W_1 and W_2 under the primary drag ×2 scenario.

Station	Depth (m)	FTIR-corrected abundance (items/L)	Particles (n)	Group-weighted mean sinking velocity (m/d)	Total modelled transport potential (items/m^2/d)	Fiber transport potential (items/m^2/d)	Non-fiber transport potential (items/m^2/d)
W_1	0	2.0	21	7.2	1.4×10^4	0.1×10^4	1.3×10^4
	10	3.1	34	21.8	6.8×10^4	0.5×10^4	6.3×10^4
	20	1.0	11	11.1	1.2×10^4	0.3×10^4	0.8×10^4
	30	2.8	30	9.2	2.6×10^4	0.9×10^4	1.7×10^4
	50	2.0	23	10.8	2.2×10^4	0.9×10^4	1.3×10^4
	75	1.5	17	9.4	1.4×10^4	0.6×10^4	0.8×10^4
	100	1.3	14	15.6	2.0×10^4	0.3×10^4	1.7×10^4
	150	1.8	19	12.2	2.2×10^4	0.4×10^4	1.7×10^4
	200	4.1	44	11.3	4.6×10^4	0.8×10^4	3.9×10^4
	250	1.9	20	18.4	3.5×10^4	0.3×10^4	3.3×10^4
	300	2.7	30	21.4	5.7×10^4	0.5×10^4	5.2×10^4
	400	2.2	23	9.0	2.0×10^4	0.3×10^4	1.7×10^4
	500	3.9	42	10.3	4.0×10^4	0.5×10^4	3.5×10^4
	600	1.3	14	4.3	0.6×10^4	0.1×10^4	0.4×10^4
	700	1.4	16	14.0	2.0×10^4	0.1×10^4	1.9×10^4
	800	1.9	20	6.1	1.1×10^4	0.4×10^4	0.7×10^4
	900	1.6	17	6.2	1.0×10^4	0.2×10^4	0.8×10^4
	1000	0.9	9	4.5	0.4×10^4	0.2×10^4	0.2×10^4
	1500	0.7	8	8.8	0.6×10^4	0.08×10^4	0.5×10^4
	2000	1.2	12	7.4	0.8×10^4	0.2×10^4	0.7×10^4
	3000	1.0	11	5.1	0.5×10^4	0.2×10^4	0.3×10^4
	4000	1.0	10	22.2	2.1×10^4	0.09×10^4	2.0×10^4
	5000	1.3	15	63.8	8.2×10^4	0.1×10^4	8.1×10^4
	5650	0.8	9	17.5	1.4×10^4	0.07×10^4	1.4×10^4
W_2	0	3.7	82	24.0	8.9×10^4	1.2×10^4	7.6×10^4
	10	2.2	54	36.4	8.0×10^4	0.7×10^4	7.4×10^4
	20	1.7	47	34.5	5.8×10^4	0.3×10^4	5.5×10^4
	30	2.1	84	27.2	5.8×10^4	1.1×10^4	4.7×10^4
	50	2.1	73	24.9	5.2×10^4	0.9×10^4	4.3×10^4
	75	0.8	53	30.3	2.4×10^4	0.2×10^4	2.3×10^4
	100	1.8	45	23.6	4.3×10^4	1.0×10^4	3.3×10^4
	150	1.2	32	13.2	1.6×10^4	0.6×10^4	1.0×10^4
	200	1.3	33	23.5	3.0×10^4	0.3×10^4	2.6×10^4
	250	0.7	39	66.9	4.8×10^4	0.1×10^4	4.7×10^4
	300	1.6	58	24.5	4.0×10^4	0.3×10^4	3.6×10^4
	400	0.7	37	16.4	1.1×10^4	0.2×10^4	1.0×10^4
	500	1.6	46	26.1	4.1×10^4	0.3×10^4	3.8×10^4
	600	1.8	60	7.2	1.3×10^4	0.5×10^4	0.8×10^4
	700	1.5	45	12.9	2.0×10^4	0.2×10^4	1.8×10^4
	800	1.4	46	13.0	1.8×10^4	0.2×10^4	1.5×10^4
	900	0.8	41	14.6	1.2×10^4	0.1×10^4	1.0×10^4
	1000	1.4	44	19.6	2.8×10^4	0.3×10^4	2.5×10^4
	1500	1.3	42	16.0	2.1×10^4	0.1×10^4	2.0×10^4

2000	1.8	62	15.1	2.8×10^4	0.2×10^4	2.5×10^4
3000	1.4	48	13.4	1.9×10^4	0.2×10^4	1.7×10^4
4000	1.1	51	14.1	1.5×10^4	0.2×10^4	1.3×10^4
5000	0.6	41	9.9	0.6×10^4	0.1×10^4	0.4×10^4
5650	0.4	41	11.7	0.4×10^4	0.04×10^4	0.4×10^4

Note: Fibers and non-fiber particles were modeled separately using morphology-specific geometries and drag corrections. Non-fiber particles were represented by projected-area-equivalent radii derived from their measured long and short axes, whereas fibers were represented using their measured length, diameter, and aspect ratio. All estimates correspond to the primary drag ×2 scenario. Visually determined abundances were corrected using the profile-specific fractions of FTIR-confirmed synthetic particles, and polymer distributions were used to constrain particle-density assignments. Rayon, cellophane, and other non-synthetic particles were excluded. The group-weighted mean sinking velocity represents the depth-specific mean obtained by weighting the modelled mean velocities of fibers and non-fiber particles according to their relative abundances. Total modelled transport potential is the sum of the fiber and non-fiber components. All 48 depth-level records were audited against Equation (4), and the total values were checked against the corresponding morphology-specific components after calculation using unrounded values. These values are transport potentials under assumed free-particle settling and are not direct measurements of depositional flux, burial flux, resuspension, or retention efficiency.

Table S5. Sensitivity of pooled modelled free-particle transport potential to the drag multiplier.

Drag scenario	Number of depth levels	Mean modelled transport potential (items/m^2/d)	Median	Minimum	Maximum
Drag ×1.5	48	3.77×10^4	2.72×10^4	5.23×10^3	1.19×10^5
Drag ×2	48	2.82×10^4	2.04×10^4	3.92×10^3	8.89×10^4
Drag ×3	48	1.88×10^4	1.36×10^4	2.61×10^3	5.93×10^4

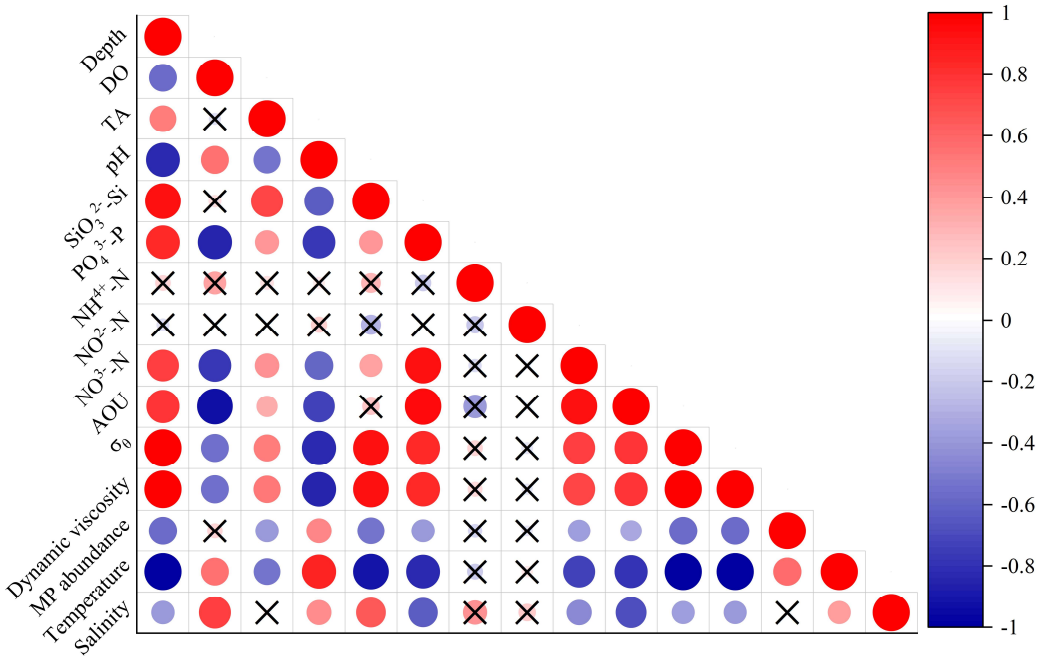


Figure S1 Spearman correlation matrix of microplastic abundance and hydrographic and biogeochemical variables in the water column of the western Pacific Pigafetta Basin. Data from the W_1 and W_2 water-column profiles were included in the analysis. Circle color represents the direction and magnitude of the Spearman's rank correlation coefficient (r), with red and blue indicating positive and negative correlations, respectively. Circle size is proportional to the absolute value of r. Crosses indicate statistically nonsignificant correlations ($p \geq 0.05$). DO, dissolved oxygen; TA, total alkalinity; AOU, apparent oxygen utilization; σ_θ, potential density anomaly; MP, microplastic.

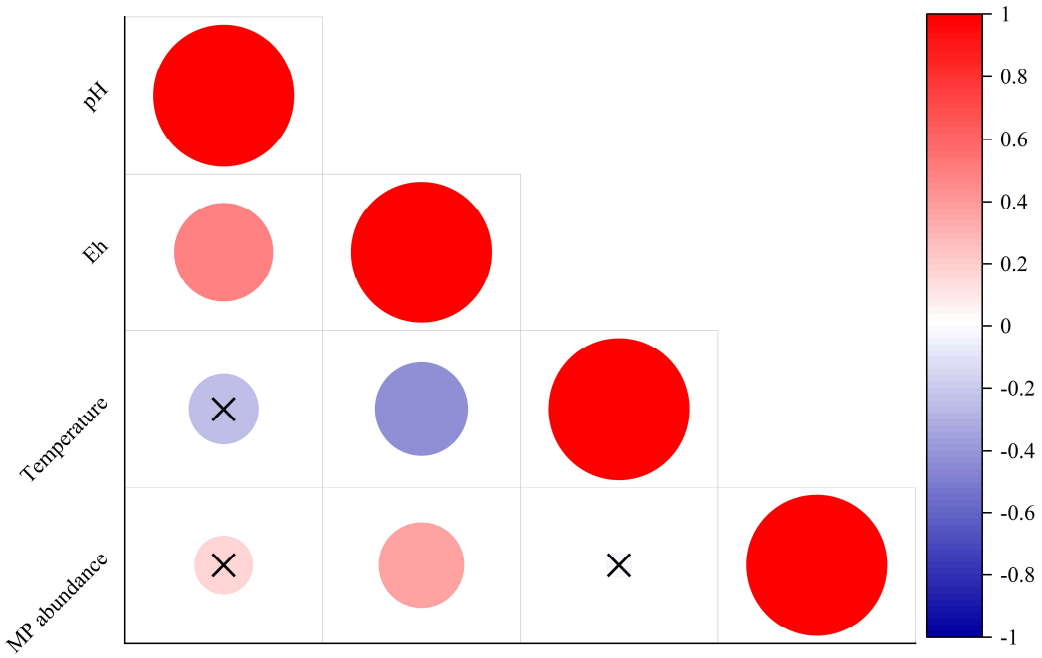


Figure S2 Spearman correlation matrix of microplastic abundance and physicochemical properties of surface sediments in the western Pacific Pigafetta Basin. Circle color represents the direction and magnitude of the Spearman's rank correlation coefficient (r), with red and blue indicating positive and negative correlations, respectively. Circle size is proportional to the absolute value of r. Crosses indicate statistically nonsignificant correlations ($p \geq 0.05$). Eh, sediment redox potential; MP, microplastic. Temperature refers to the temperature during sediment physicochemical measurements.